Available online at www.sciencedirect.com

ScienceDirect

IFAC PapersOnLine 53-1 (2020) 81–86

IFAC Papers Online CONFERENCE PAPER ARCHIVE

Autonomous Landing Design of UAVs using Feedback Linearization Controller with Anti Windup Scheme

Amit Kumar Tripathi * **Vijay V Patel** * **Radhakant Padhi** **

* *Scientist, Aeronautical Development Agency, Bangalore, India.*
** *Professor, Indian Institute of Science, Bangalore, India. (E-mail: padhi@iisc.ac.in)*

Abstract: This paper presents autonomous landing controller design of unmanned aerial vehicles (UAVs). Feedback linearization approach with anti windup scheme is designed as autonomous landing controller. Anti windup basically controls the integrator component accumulation in the autopilot design and restricts the output within saturation limits. Autonomous landing of a fixed wing UAV consists of approach, glideslope and flare phases. During approach, aerial vehicle aligns itself with runway and reduces its lateral deviations with respect to runway central line. In glide slope phase, aerial vehicle maintains a fixed flight path angle and descends with a constant sink rate. In flare phase, aerial vehicle follows an exponential trajectory and descends with a lower sink rate which keeps reducing further as it goes to lower altitudes. Flare controller is designed with integrator and antiwindup scheme is used to handle the controller output within saturation limits. Landing is primarily a longitudinal mode operation but due to disturbances and coupling lateral and directional modes also gets activated. In this paper pitch angle, roll angle and yaw angle nonlinear dynamic equations are linearized to obtain the control commands in terms of elevator deflection, aileron deflection and rudder deflections. Similarly total velocity of aerial vehicle being an important parameter is controlled using thrust command. A first order linearized model of velocity is used to obtain thrust control command. Autonomous landing of UAV with feedback linearization controller and anti windup scheme is simulated with Six-DOF model of AE2 UAV. The algorithm is implemented with wind disturbances to show the autonomous landing performance of UAV.

Keywords: Feedback Linearization, glideslope, flare, anti windup, landing, unmanned aerial vehicle, touchdown point, sink rate

1. INTRODUCTION

The autonomous landing plays a very important role for UAVs. The landing phase of flight is considered as one of the most critical phase as it requires precision and smoothness and minimum delay. During landing, a UAV is severely affected by the external disturbances such as crosswinds, wind shear and the ground effects. It is required to design the efficient controllers which can take care of all the effects and provide a designated touchdown point landing. The Autonomous landing comprise of mainly three phases Prasad and Pradeep (2007) such as alignment and approach phase, where UAV aligns with the runway by correcting the heading. Next is glideslope phase, where the UAV follows a fixed ramp path with constant flight path angle until it reaches a flare height. During the glideslope phase UAV descends with a higher sink rate. Once the flare height is achieved the UAV follows a exponential trajectory until the touchdown point. During the flare trajectory the UAV is closer to ground, sink rate is reduced and the UAV descends under stricter controller requirements than the glideslope phase. Flare is an important phase of UAV and the altitude control should be very efficient as well as ground effects Military (1980) are also dominant in this phase. The different phases of autolanding is shown in Fig. (1).

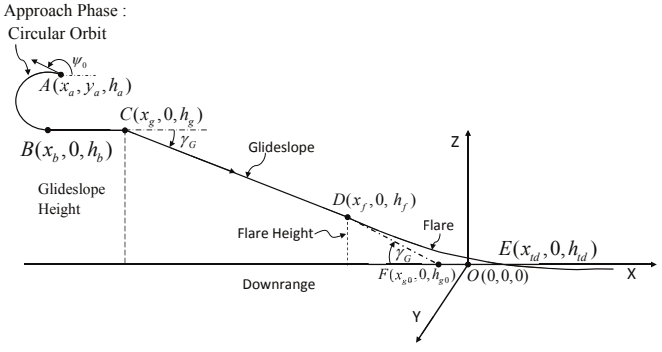

Fig. 1. Autonomous landing Phases of an Unmanned Aerial Vehicle

Different control theories that address the auto-landing problem are available in the literature. Nonlinear controllers with Feedback linearization Prasad and Pradeep (2007); Atmeh et al. (2011); Wagner and Valasek (2007) are used for auto landing problem. Automatic landing system design using fuzzy logic has been proposed in Nho and Agarwal (2000). In this paper, feedback linearization controller is used to perform autonomous landing of a UAV. Feedback linearization controller provides good tracking and also provides robustness. Feedback linearization controllers can be tuned to handle certain un-

2405-8963
Peer review under responsibility of International Federation of Automatic Control.
10.1016/j.ifacol.2020.06.014

certainties or disturbances. Autolanding Strategies for a Fixed Wing UAV in Adverse Atmospheric Conditions has been proposed in Yavrucuk and Kargin (2008).

2. MATHEMATICAL MODEL OF UAV

2.1 Nonlinear UAV State Dynamics

Assuming airplane to be a rigid body and earth to be flat the complete set of Six Degree of Freedom (Six-DOF) equations are provided in Stevens and Lewis (2003); Roskam (2003); Roskam and Lan (1997). In the present work Six-DOF state dynamics model of AE-2 UAV is considered based on forces and moments acting on the UAV.

$$\dot{u} = rv - qw - g\sin\theta + X_a + X_t \tag{1}$$
$$\dot{v} = pw - ru + g\sin\phi\cos\theta + Y_a \tag{2}$$
$$\dot{w} = qu - pv + g\cos\phi\cos\theta + Z_a \tag{3}$$
$$\dot{p} = c_1 rq + c_2 pq + c_3 L_a + c_4 N_a \tag{4}$$
$$\dot{q} = c_5 pr + c_6(p^2 - r^2) + c_7(M_a + M_t) \tag{5}$$
$$\dot{r} = c_8 pq - c_2 rq + c_4 L_a + c_9 N_a \tag{6}$$
$$\dot{\phi} = p + q\sin\phi\tan\theta + r\cos\phi\tan\theta \tag{7}$$
$$\dot{\theta} = q\cos\phi - r\sin\phi \tag{8}$$
$$\dot{\psi} = q\sin\phi\sec\theta + r\cos\phi\sec\theta \tag{9}$$
$$\dot{x} = u\cos\theta\cos\psi + v(\sin\phi\sin\theta\cos\psi - \cos\phi\sin\psi) + w(\cos\phi\sin\theta\cos\psi + \sin\phi\sin\psi) \tag{10}$$
$$\dot{y} = u\cos\theta\sin\psi + v(\sin\phi\sin\theta\sin\psi + \cos\phi\cos\psi) + w(\cos\phi\sin\theta\sin\psi - \sin\phi\cos\psi) \tag{11}$$
$$\dot{h} = u\sin\theta - v\sin\phi\cos\theta - w\cos\phi\cos\theta \tag{12}$$

where u, v, w are velocity components and p, q, r are roll, pitch and yaw rates respectively about the body axis. ϕ, θ, ψ are Euler angles and h is the height above ground. x is forward distance and y is sideward distance. X_a, Y_a, Z_a are the aerodynamic forces per unit mass and L_a, M_a, N_a are the aerodynamic moments about the body axis. X_t is the force per unit mass in direction X due to thrust and M_t is the moment around the Y axis caused by thrust offset from the center of gravity (CG) of the UAV. The coefficients $c_1 - c_9$ are functions of moment of inertia I_{xx}, I_{yy}, I_{zz} and I_{xz} as provided in Stevens and Lewis (2003).

In the translational dynamic Eqs.(1-3) u, v and w can also be written as follows

$$u = V_T\cos\alpha\cos\beta,\ v = V_T\sin\beta,\ w = V_T\sin\alpha\cos\beta \tag{13}$$

Where, total speed V_T, angle of attack α and angle of side slip β can be written as follows

$$\dot{V}_T = \frac{u\dot{u} + v\dot{v} + w\dot{w}}{V_T} \tag{14}$$
$$\dot{\alpha} = \frac{u\dot{w} - w\dot{u}}{u^2 + w^2},\ \dot{\beta} = \frac{\dot{v}\left(u^2 + w^2\right) - V\left(u\dot{u} + w\dot{w}\right)}{{V_T}^2\sqrt{(u^2 + w^2)}} \tag{15}$$

2.2 Aerodynamic Forces and Moments

The aerodynamic body axis forces: X_a, Y_a and Z_a and aerodynamic moments: roll moment L_a, pitch moment M_a, and yaw moment N_a are given as follows

Table 1. Physical data of AE-2

b m	c m	m kg	I_{xx} kgm^2	I_{yy} kgm^2	I_{zz} kgm^2	I_{xz} kgm^2
2	0.3	6	0.5062	0.89	0.91	0.0015

$$[X_a\ \ Y_a\ \ Z_a] = \frac{\overline{q}S}{m}[C_X\ \ C_Y\ \ C_Z] \tag{16}$$
$$[L_a\ \ M_a\ \ N_a] = \overline{q}S[bC_l\ \ cC_m\ \ bC_n] \tag{17}$$

where, C_X is body X- axis force coefficient, C_Y is body Y-axis force coefficient, C_Z is body Z-axis force coefficient. C_m is pitching moment coefficient, C_l is rolling moment coefficient, C_n is yawing moment coefficient. $\overline{q}$ is dynamic pressure and S is wing planform area. b is wing span and c is chord length. Aerodynamic coefficients obtained from curve fitting on wind tunnel data Singh and Padhi (2009) are given as follows

$$C_X = C_{X_0} + C_{X_\alpha}(\alpha)\alpha + C_{X_{\delta e}}(\alpha)\delta e + C_{X_Q}(\alpha)\bar{q}$$
$$C_Y = C_{Y_\beta}(\alpha)\beta + C_{Y_{\delta a}}(\alpha)\delta a + C_{Y_{\delta r}}(\alpha)\delta r + C_{Y_P}(\alpha)\bar{p} + C_{Y_R}(\alpha)\bar{r}$$
$$C_Z = C_{Z_0} + C_{Z_\alpha}(\alpha)\alpha + C_{Z_\beta}\beta + C_{Z_{\delta e}}\delta e + C_{Z_Q}(\alpha)\bar{q}$$
$$C_l = C_{l_\beta}(\alpha)\beta + C_{l_{\delta a}}(\alpha)\delta a + C_{l_P}(\alpha)\bar{p} + C_{l_R}(\alpha)\bar{r}$$
$$C_m = C_{m_0} + C_{m_\alpha}(\alpha)\alpha + C_{m_\beta}(\alpha,\beta)\beta + C_{m_{\delta e}}(\alpha)\delta e + C_{m_Q}(\alpha)\bar{q}$$
$$C_n = C_{n_\beta}(\alpha)\beta + C_{n_{\delta r}}(\alpha)\delta r + C_{n_P}(\alpha)\bar{p} + C_{n_R}(\alpha)\bar{r}$$

where,

$$[\bar{p}\ \ \bar{q}\ \ \bar{r}] = \frac{1}{2V_T}[bp\ \ \ cq\ \ \ br]$$

where α is angle of attack and β is side slip angle. δa, δe, δr are aileron, elevator and rudder control deflections respectively. Static and dynamic derivatives are functions of α and β. Static tests were conducted in wind tunnel. The dynamic derivatives are computed with Athennae Vortex Lattice (AVL) software Singh and Padhi (2009).

2.3 The UAV Aerodynamic Model

It is designed and developed at UAV lab of aerospace engineering department, IISc. AE-2 is a fixed wing airplane designed for autonomous flying. It has been designed for long endurance, where the flight duration is expected to be around 45 minutes. The thrust generating unit of the AE-2 is an electric motor with propeller, which is powered by lithium-polymer battery. It has a pusher configuration of thrust, this has been done so that gimballed camera can be mounted at the nose. The physical data of AE-2 is given in Table 1.

Thrust Control Thrust command is used to control the velocity. Initially the velocity and thrust is set at trim values.

$$T = T_{max}\sigma_t, X_t = \frac{T}{m}, M_t = -Td \tag{18}$$

where T is the engine thrust, σ_t is the control input for engine thrust. M_t is moment due to engine thrust and d is offset of the engine thrust force from the center of gravity.

Initial Trim Condition The $AE-2$ initial conditions are computed by solving the nonlinear dynamic equations for a particular trim condition are provided in Table 2.

Table 2. Trim data of AE-2

α	θ	q	δ_e	σ_t	V_T	h
3.134°	3.134°	$0°/s$	$-3.267°$	0.371	$20m/s$	$100m$

3. PATH PLANNIG AND GUIDANCE DESIGN FOR AUTOMATIC LANDING

The Auto landing maneuver has three important phases 1. Approach phase 2. glideslope phase and 3. flare phase. All the three phases are described in the following subsections

3.1 Auto-Landing with Feedback Linearization Controller

Flight dynamics equations Eq.(1) to Eq.(12) can be represented by following equation in a compact form

$$\dot{X} = f(X) + g(X)U \tag{19}$$

where $X = [u, v, w, p, q, r, \phi, \theta, \psi, x, y, z]$ are the states of the flight dynamics model and $U = [\sigma_t, \delta_e, \delta_a, \delta_r]$ are control inputs of the flight dynamics model. All the notations have standard meaning. Feedback linearization in general deals with the feedback control signal U which can transform a nonlinear system into an equivalent linear system.

Typical feedback control input signal for aforementioned dynamic model is provided as follows.

$$U = g(X)^{-1}(L_M - f(X)) \tag{20}$$

Where, L_M is the linearized or approximated linear model of the plant shown in Eq.(19). In this paper nonlinear dynamics of $\ddot{\phi}$, $\ddot{\theta}$ and $\ddot{\psi}$ are approximated using feedback linearization and L_M is designed as per Eq.(26) to Eq.(28) respectively.

In the present work roll angle ϕ, pitch angle θ and yaw angle ψ kinematic equations represented by Eq. (7) to Eq. (9) are differentiated. The differentiated equations contain the terms roll rate $\dot{p}$, pitch rate $\dot{q}$ and yaw rate $\dot{r}$ which are substituted from Eq. (4) to Eq. (6). Thus the following model equation (21) in feedback linearization framework can be obtained.

$$\ddot{Y}_l = F_l(x_l) + G_l(x_l)u_l \tag{21}$$

where, $Y_l = [\phi, \theta, \psi]$, $x_l = [\phi, \theta, \psi, p, q, r]$ and $u_l = [L, M, N]$. Where, L, M and N are roll moment, pitch moment and yaw moment of the aircraft. The expression of $F_l(x_l) = [f_{l1}(x_l), f_{l2}(x_l), f_{l3}(x_l)]$ is provided as follows.

$$\begin{aligned} f_{l1}(x_l) = {} & q(\cos\phi\tan\theta(p + r\cos\phi\tan\theta + q\sin\phi\tan\theta) \\ & + \sin\phi(1 + (\tan\theta)^2)(q\cos\phi - r\sin\phi)) \\ & + r(-\sin\phi\tan\theta(p + r\cos\phi\tan\theta + q\sin\phi\tan\theta) \\ & + \cos\phi(1 + (tan\theta)^2)(q\cos\phi - r\sin\phi)) \\ & + (c_1 r + c_2 p)q + \sin\phi\tan\theta(c_5 pr - c_6(p^2 - r^2)) \\ & + \cos\phi\tan\theta(c_8 p - c_2 r)q \end{aligned} \tag{22}$$

$$\begin{aligned} f_{l2}(x_l) = {} & -q(p + r\cos\phi\tan\theta + q\sin\phi\tan\theta) - r\cos\phi \\ & (p + r\cos\phi\tan\theta + q\sin\phi\tan\theta) + \cos\phi \\ & (c_5 pr - c_6(p^2 - r^2)) - \sin\phi(c_8 p - c_2 r)q \end{aligned} \tag{23}$$

$$\begin{aligned} f_{l3}(x_l) = {} & q(\cos\phi\sec\theta(p + r\cos\phi\tan\theta + q\sin\phi\tan\theta) \\ & + \sin\phi\sec\theta\tan\theta(q\cos\phi - r\sin\phi)) \\ & + r(-\sin\phi\sec\theta(p + r\cos\phi\tan\theta + q\sin\phi\tan\theta) \\ & + \cos\phi\sec\theta\tan\theta(q\cos\phi - r\sin\phi)) \\ & + \sin\phi\sec\theta(c_5 pr - c_6(p^2 - r^2)) + \cos\phi\tan\theta \\ & (c_8 P - c_2 r)q \end{aligned} \tag{24}$$

The expression of $G_l(x_l)$ is provided as per Eq. (25).

$$G_l(x_l) = \begin{bmatrix} c_3 + c_4\cos\phi\tan\theta & c_7\sin\phi\tan\theta & c_4 + c_9\cos\phi\tan\theta \\ -c_4\sin\phi & c_7\cos\phi & -c_9\sin\phi \\ c_4\cos\phi\sec\theta & c_7\sin\phi\sec\theta & c_9\cos\phi\sec\theta \end{bmatrix} \tag{25}$$

The approximate model $Y_a = [Y_{a1}, Y_{a2}, Y_{a3}]$ for Eq. (21) can be written as follows

$$\ddot{Y}_{a1} = -k_{\dot{\phi}}\dot{\phi} - k_{\phi}(\phi - \phi_d) \tag{26}$$

$$\ddot{Y}_{a2} = -k_{\dot{\theta}}\dot{\theta} - k_{\theta}(\theta - \theta_d) \tag{27}$$

$$\ddot{Y}_{a3} = -k_{\dot{\psi}}\dot{\psi} - k_{\psi}(\psi - \psi_d) \tag{28}$$

Where, $k_{\dot{\phi}}$, $k_{\dot{\theta}}$ and $k_{\dot{\psi}}$ are feedback linearization derivative gains and k_{ϕ}, k_{θ} and k_{ψ} are proportional gains. Equating model equations and approximated model equations, the control commands are computed in terms of ϕ_d, θ_d and ψ_d. The pitch, roll and yaw moments are computed as per Eq. (29).

$$u_l = (G_l(x_l))^{-1}(\ddot{Y}_a - F_l(x_l)) \tag{29}$$

In the Eq. (29) the term $\ddot{Y}_a$ is computed by substituting expressions from Eq. (26) to Eq. (28). The control commands $u = [\delta_e, \delta_a, \delta_r]$ can be computed from desired moment commands, u_l as per Eq. (30).

$$u = {G_r}^{-1}[u_l - F_r] \tag{30}$$

where, G_r is defined as follows

$$G_r = \begin{bmatrix} c_3 L_{a_u} & 0 & c_4 N_{a_u} \\ 0 & c_7 M_{a_u} & 0 \\ c_4 L_{a_u} & 0 & c_9 N_{a_u} \end{bmatrix} \tag{31}$$

where, L_{a_u}, M_{a_u} and N_{a_u} are components of roll, pitch and yaw moments expression containing aileron, elevator and rudder surface deflection terms respectively and defined as follows.

$$L_{a_u} = \hat{q}SbC_{l_{\delta a}},\ M_{a_u} = \hat{q}ScC_{l_{\delta e}},\ N_{a_u} = \hat{q}SbC_{l_{\delta r}} \tag{32}$$

F_r is defined as follows

$$F_r = \begin{bmatrix} L_{a_x} \\ (M_{a_x} + M_t) \\ N_{a_x} \end{bmatrix} \tag{33}$$

where, L_{a_x}, M_{a_x} and N_{a_x} are complementary components of roll, pitch and yaw moments expression respectively without aileron, elevator and rudder surface deflection terms and are defined as follows.

$$L_{a_x} = \hat{q}Sb\left[C_{l_\beta}(\alpha)\beta + C_{l_P}(\alpha)\bar{p} + C_{l_R}(\alpha)\bar{r}\right] \tag{34}$$

$$M_{a_x} = \hat{q}Sc\left[m_0 + C_{m_\alpha}(\alpha)\alpha + C_{m_\beta}(\alpha,\beta)\beta + C_{m_Q}(\alpha)\bar{q}\right] \tag{35}$$

$$N_{a_x} = \hat{q}Sb\left[C_{n_\beta}(\alpha)\beta + C_{n_P}(\alpha)\bar{p} + C_{n_R}(\alpha)\bar{r}\right] \tag{36}$$

In present work $\phi_d = 0$ and $\psi_d = 0$ is considered. The expression for θ_d is computed in the following sections for glideslope mode controller and flare mode controller.

Approach Phase Approach phase as shown in Fig. (1) is usually heading alignment phase where the UAV aligns with the runway. Once the UAV aligns with the runway it is basically level flying phase until glideslope descent begins.

Glideslope Controller Design In the glideslope descent phase of autonomous landing, UAV has to follow a constant glideslope reference trajectory. The typical reference angle γ_G is desired glideslope angle along the glidepath and it is typically in

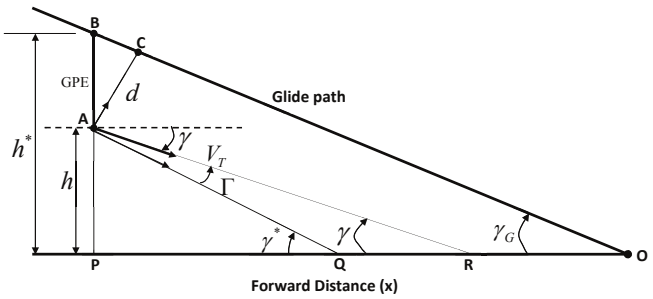

Fig. 2. Glideslope Altitude and Gamma Error Computation

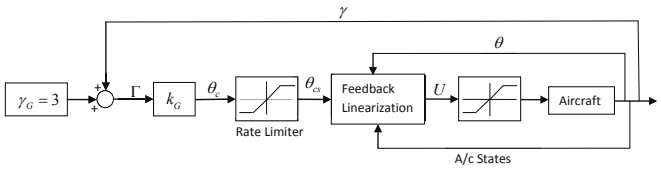

Fig. 3. Glideslope autopilot block diagram

the range of $2.5^\circ - 3.5^\circ$ deg. The error between flight path angle γ and glideslope angle γ_G is represented as Γ and computed as per Eq.(37).

$$\Gamma = \gamma - \gamma_G \tag{37}$$

Flight path angle error Γ is shown in Fig. (2). Flight path error corresponds to glide path error (GPE) as shown in Fig. (2). It can be noticed that h^* is the desired altitude and h is the current altitude of aircraft and $GPE = h^* - h$. The glidepath deviation is defined as perpendicular distance of the aircraft position from glideslope reference γ_G trajectory as described in Nho and Agarwal (2000). Glidepath deviation rate $\dot{d}$ is defined as component of velocity perpendicular to reference glideslope line from the aircraft position. Glidepath deviation rate from fixed γ_G reference line is computed with a constraint ($\dot{\gamma} = 0$) as per Eq. (38).

$$\dot{d} = V_T \sin(\gamma - \gamma_G) \tag{38}$$

Commanded pitch angle is defined as a function of glideslope deviation. Commanded pitch angle can be provided as per Eq.(39) where, k_G is glideslope feedback linearization controller gain. Glideslope autopilot block diagram is shown in Fig. (3).

$$\theta_c = -k_G(\gamma - \gamma_G) \tag{39}$$

Where θ_c is the glide slope controller demand as per Eq.(39) and it is substituted in Eq.(27). A rate limiter is added to obtain θ_{cs}. This commanded value of θ_{cs} is actually fed to the feedback linearization controller.

Flare Controller Design Flare starts from flare initiation point $h(0)$ or flare height h_f. During flare, UAV follows exponential trajectory. Flare height can be computed from the descent rate.

$$h(t) = h(0)\exp^{-t/\tau} - 1 = h_f \exp^{-t/\tau} - 1 \tag{40}$$

where τ is time constant. The commanded height h_d can be given as

$$h_d = h_f \exp^{-t/\tau} - 1 \tag{41}$$

Differentiating Eq. (41) with respect to t, Eq. (42) is obtained

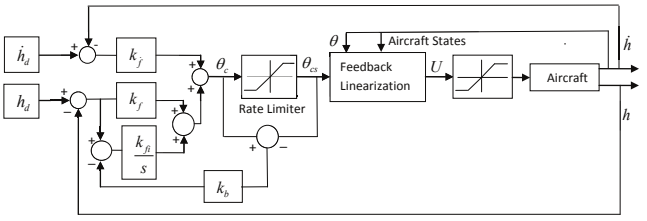

Fig. 4. Flare autopilot block diagram with Anti Windup

$$\dot{h}_d = -h_f \frac{\exp^{-t/\tau}}{\tau} = -\frac{h_d + 1}{\tau} \tag{42}$$

Sink rate can also be computed from vehicle trajectory profile with known velocity and glide slope angle as follows

$$\dot{h} = V_T \sin\gamma \tag{43}$$

Flare height can be computed by equating Eq. (42) and Eq. (43) and computing h_d based on appropriate flight condition and time constant.

Altitude h and Z (in NED coordinate frame), sink rate $\dot{h}$ are measured from system dynamical equations as follows

$$h = -Z,\ \dot{h} = -\dot{Z},\ \dot{Z} = -V\sin\gamma \tag{44}$$

The flare controller computes desired pitch angle command as per Eq. (45) which is a function of altitude and sink rate

$$\theta_c = -k_f(h - h_d) - k_{\dot{f}}(\dot{h} - \dot{h}_d) - k_{fi}\int (h - h_d + k_b(\theta_c - \theta_{cs}))dt \tag{45}$$

Flare autopilot block diagram as shown in Fig. (4). Where, k_f and $k_{\dot{f}}$ are flare controller gains and θ_c is the flare controller demand as per Eq.(45) and it is substituted in Eq.(27). A rate limiter is added to obtain θ_{cs}. This commanded value of θ_{cs} is actually fed to the feedback linearization controller. A tracking anti windup loop is added in the flare block diagram with feedback gain k_b. Anti windup scheme is presented in Bohn and Atherton (1995) and Ghoshal and John (2010). Anti windup scheme provides reduction in the rate of integrator output increase. Flare controller is designed by tuning gains so that desired altitude and sink rate can be achieved simultaneously.

3.2 Thrust Controller

Total velocity of the unmanned aerial vehicle (UAV) is controlled by thrust control command. A first order error function on velocity is represented as per Eq. (46)

$$\dot{V}_T = -K_{V_T}(V_T - V_{td}) \tag{46}$$

Where, K_{V_T} is first order error function gain and V_{td} is the desired total speed. The following expression can be obtained by substituting u, v and w from Eq. (13) in Eq. (14).

$$\dot{V}_T = \dot{u}\cos\alpha\cos\beta + \dot{v}\sin\beta + \dot{w}\sin\alpha\cos\beta \tag{47}$$

Thrust command is computed by equating Eq. (46) with total velocity dynamics provided in Eq. (47). It can be noticed from translational flight dynamics equations Eq. (1) - Eq. (3) and Eq. (18) that only $\dot{u}$ is function of thrust. Therefore, $\dot{u}$ can be obtained as follows

$$\dot{u} = -\frac{K_{V_T}(V_T - V_{td}) + \dot{v}\sin\beta + \dot{w}\sin\alpha\cos\beta}{\cos\alpha\cos\beta} \tag{48}$$

Further, Eq. (48) can be simplified to obtain thrust command using Eq. (1) and Eq. (18) as follows

$$X_t = -\frac{K_{V_T}(V_T - V_{td}) + \dot{v}\sin\beta + \dot{w}\sin\alpha\cos\beta}{\cos\alpha\cos\beta} - rv + qw + g\sin\theta - X_a \quad (49)$$

Further simplification using Eq. (18) leads to thrust command as follows

$$\sigma_t = -\frac{m(K_{V_T}(V_T - V_{td}) + \dot{v}\sin\beta + \dot{w}\sin\alpha\cos\beta)}{T_{max}\cos\alpha\cos\beta} - \frac{m(rv - qw - g\sin\theta + X_a)}{T_{max}} \quad (50)$$

Further rearrangement leads to following equation for thrust control command σ_t.

$$\sigma_t = -\frac{m(K_{V_T}(V_T - V_{td}))}{T_{max}\cos\alpha\cos\beta} - \frac{m\dot{v}\sin\beta}{T_{max}\cos\alpha\cos\beta} - \frac{m\dot{w}\sin\alpha\cos\beta}{T_{max}\cos\alpha\cos\beta} - \frac{m(rv - qw - g\sin\theta + X_a)}{T_{max}} \quad (51)$$

Substituting $\dot{v}$ from Eq.(2) and $\dot{w}$ from Eq.(3), the following expression shown in Eq.(52) for thrust control command σ_t can be obtained.

$$\sigma_t = -\frac{m(K_{V_T}(V_T - V_{td}))}{T_{max}\cos\alpha\cos\beta} + \frac{m(ru - g\sin\phi\cos\theta - Y_a)\sin\beta}{T_{max}\cos\alpha\cos\beta} - \frac{m(qu + g\cos\phi\cos\theta + Z_a)\sin\alpha\cos\beta}{T_{max}\cos\alpha\cos\beta} - \frac{m(rv - qw - g\sin\theta + X_a)}{T_{max}} \quad (52)$$

Thrust control command is provided in Eq. (52) to control total speed V_T of UAV to a desired total speed V_{td}. It can also be noticed that angle of attack $\alpha = 90\,deg$ and angle of sideslip $\beta = 90\,deg$ values can be avoided in order to avoid singularity condition in thrust control command.

4. SIMULATION RESULTS

This section presents the simulation results for autonomous landing of a UAV with feedback linearization controller. Glideslope controller is designed using gamma control . Flare controller is designed using altitude and sink rate control. The initial states are set to the trim conditions. Feedback linearization controller tracks the reference trajectory. The autonomous landing trajectory of UAV is shown in Fig. (5). Initial position of trajectory is $X_i = [-1500, 0, 100]$. Initial phase is level flying phase after that it undergoes glideslope and then flare phases. At touchdown point, final position is $X_f = [524, 0, 0]$.

The longitudinal states of UAV during autonomous landing are shown in Fig. (6). It can be noticed that at time $t = 20\,sec$, angle of attack α, pitch angle θ and pitch rate Q observe transients due to change of level phase to glideslope phase. Total Speed $V_t = 22\,m/s$ is kept constant during autonomous landing maneuver. At time $t = 70\,sec$, UAV enters into flare mode from glide slope phase. Flare mode starts at flare height $h_f = 11.76\,m$. The altitude during the flight time is shown in Fig. (6). It begins from trim altitude of $100\,m$ then UAV undergoes glideslope mode and follows a ramp profile until the altitude of $11.76\,m$. It follows exponential profile during the flare phase till touchdown. The control commands during the flight time is shown in Fig. (7). Thrust command and elevator deflection are control commands in the longitudinal axis. It can

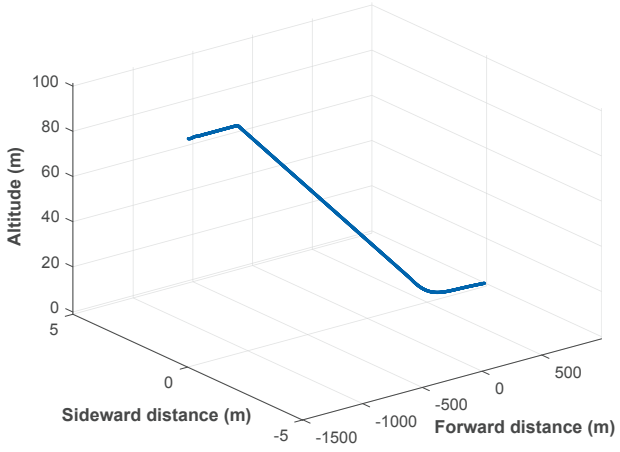

Fig. 5. Autonomous landing trajectory of UAV

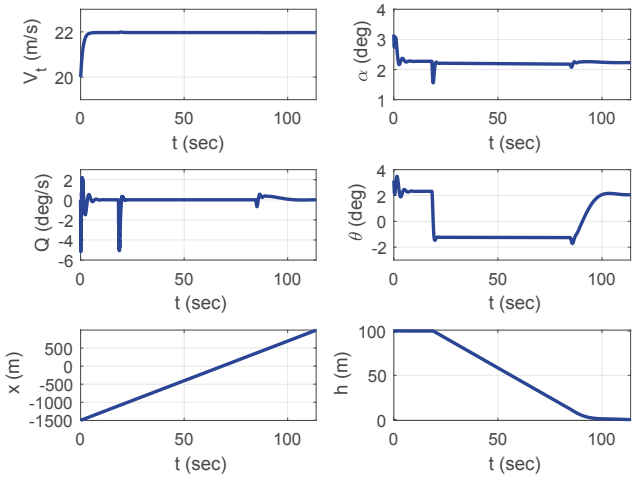

Fig. 6. Longitudinal states of autolanding UAV

be noticed that thrust and elevator deflection is constant during glideslope phase. It can also be noticed that thrust command and elevator deflection command is smoothely changing during the flare phase. However aileron and rudder deflections are used to handle the wind disturbances added in the model. Landing is predominantly a longitudinal phenomenon.

The sink rate during the flight time is shown in Fig. (8). It can be noticed that sink rate is constant during glideslope phase (sink rate $= -1.3\,m/s$). During flare phase sink rate gradually reduces till -0.1 m/s. It can be concluded that flare phase provides a smooth touchdown for the aircraft with lower on ground impact.

The flight path angle during the flight time is shown in Fig. (9). It can be noticed that at time $t = 20\,sec$ aircraft enters into glideslope mode from level flight mode $\gamma = 0\,deg$. It can be noticed that flight path angle is constant during glideslope phase $\gamma = -3.5\,deg$. During flare phase flight path angle gradually changes to zero.

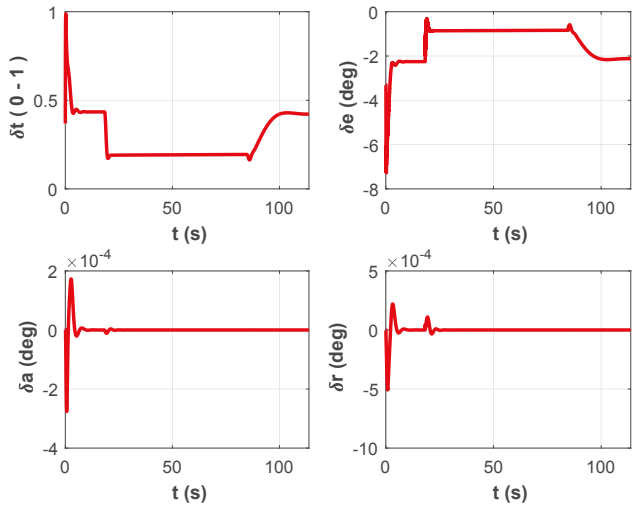

Fig. 7. Control commands of autolanding UAV

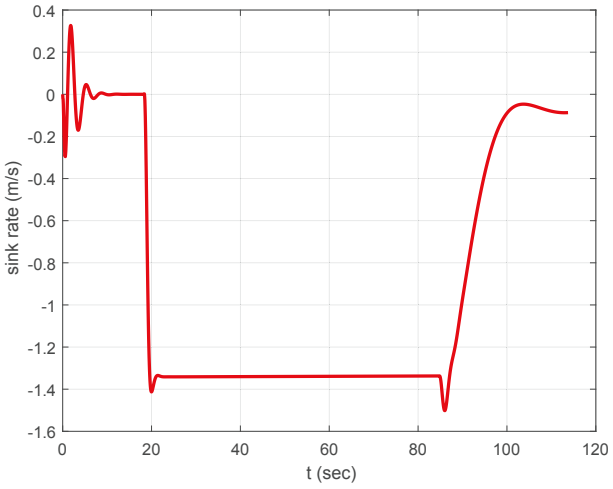

Fig. 8. Sink rate of autolanding UAV

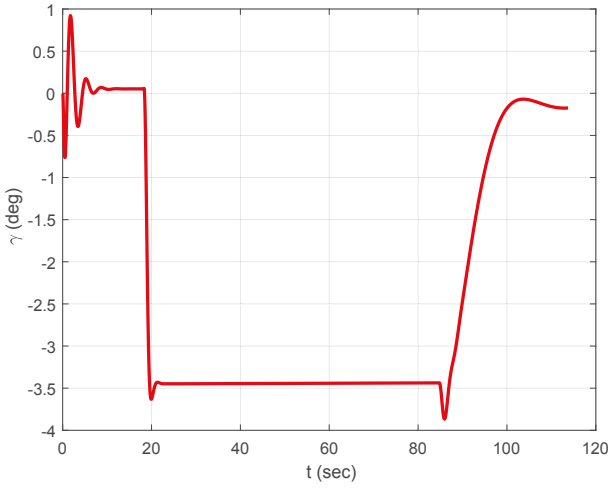

Fig. 9. Flight path angle profile of autolanding UAV

5. CONCLUSION

The autonomous landing problem for an unmanned aerial vehicle has been attempted using Six-DOF model of UAV with wind disturbances and feedback linearization with anti Windup controller. The pitch angle, roll angle and yaw angle kinematics are differentiated and their respective second order derivatives are obtained. The second order derivatives of attitude and heading angles are obtained in terms of pitch rate, roll rate and yaw rate first order derivative terms which further got simplified with appropriate substitution to incorporate control surface deflections. The nonlinear second order derivative of Euler angles are also approximated or linearized with linear models containing angle derivative, angle error terms and gains. The nonlinear second order dynamics is equated with its linear model to compute control commands. During glideslope the commanded pitch angle is presented as a function of flight path angle error and controller is tuned to achieve commanded pich angle in order to maintain the desired flight path angle. During flare phase, commanded pitch angle is presented as a function of sink rate as well as altitude error and controller is tuned to achieve commanded pich angle in order to maintain the desired exponential flare trajectory. Anti-windup scheme is used in flare design to restrict the controller output within saturation limits.

REFERENCES

Atmeh, G.M., Al-Taq, W.I., and Hasan, Z. (2011). A nonlinear automatic landing control system for a *UAV*. In *ASME 2011 International Mechanical Engineering Congress and Exposition*, 383–392. American Society of Mechanical Engineers.

Bohn, C. and Atherton, D. (1995). An analysis package comparing pid anti-windup strategies. *IEEE Control Systems Magazine*, 15(2), 34–40.

Ghoshal, A. and John, V. (2010). Anti-windup schemes for proportional integral and proportional resonant controller.

Military, U.S. (1980). U s military specification mil-f-8785c. Technical report, U S Military.

Nho, K. and Agarwal, R.K. (2000). Automatic landing system design using fuzzy logic. *Journal of Guidance, Control, and Dynamics*, 23(2), 298–304.

Prasad, B. and Pradeep, S. (2007). Automatic landing system design using feedback linearization method. In *AIAA Conference and Exhibit,7-10 May, Rohnert Park, California*, 7-10 May. AIAA Conference and Exhibit, Rohnert Park, California.

Roskam, J. (2003). *Airplane flight dynamics and automatic flight controls*. DAR Corporation.

Roskam, J. and Lan, C.T.E. (1997). *Airplane aerodynamics and performance*. DAR Corporation.

Singh, S. and Padhi, R. (2009). Automatic path planning and control design for autonomous landing of *UAVs* using dynamic inversion. In *American Control Conference, 2009. ACC'09.*, 2409–2414. IEEE.

Stevens, B. and Lewis, F. (2003). *Aircraft Control and Simulation 2nd Edition*. John Wiley & Sons.

Wagner, T. and Valasek, J. (2007). Digital autoland control laws using quantitative feedback theory and direct digital design. *Journal of Guidance, Control, and Dynamics*, 30(5), 1399–1413.

Yavrucuk, I. and Kargin, V. (2008). Autolanding strategies for a fixed wing uav in adverse atmospheric conditions. In *AIAA Guidance, Navigation and Control Conference and Exhibit*, 6963.